Song *et al. Biochar* (2024) 6:76
https://doi.org/10.1007/s42773-024-00372-9

Biochar

ORIGINAL RESEARCH Open Access

# Oyster shell facilitates the green production of nitrogen-doped porous biochar from macroalgae: a case study for removing atrazine from water

Liying Song[1†], Hu Cheng[2†], Cuiying Liu[3], Rongting Ji[4], Shi Yao[1], Huihui Cao[1], Yi Li[2], Yongrong Bian[1], Xin Jiang[1], Irmina Ćwieląg-Piasecka[5] and Yang Song[1*]

## Abstract

Low-cost and green preparation of efficient sorbents is critical to the removal of organic contaminants during water treatment. In this study, the co-pyrolysis of macroalgae and oyster shell was designed to synthesize nitrogen-doped porous biochars for sorption removal of atrazine from water. Oyster shell played a significant role in opening pores in macroalgae-derived biochars, resulting in the surface area of the macroalgae (*Enteromorpha prolifera* and *Ulva lactuca*) and oyster shell co-pyrolyzed carbonaceous as high as 1501.80 $m^2\ g^{-1}$ and 1067.18 $m^2\ g^{-1}$, the pore volume reached 1.04 $cm^3\ g^{-1}$ and 0.93 $cm^3\ g^{-1}$, and O/C decreased to 0.09 and 0.08, respectively. The sorption capacity of atrazine to nitrogen-doped porous biochars (the *Enteromorpha prolifera, Ulva lactuca* and oyster shell co-pyrolyzed carbonaceous) reached 312.06 mg $g^{-1}$ and 340.52 mg $g^{-1}$. Pore-filling, hydrogen bonding, π-π or *p*-π stacking and electrostatic interaction dominated the multilayer sorption process. Moreover, the nitrogen-doped porous biochars showed great performance in cyclic reusability, and the *Enteromorpha prolifera*, *Ulva lactuca* and oyster shell co-pyrolyzed carbonaceous sorption capacity still reached 246.13 mg $g^{-1}$ and 255.97 mg $g^{-1}$, respectively. Thus, this study suggested that it is feasible and efficient to remove organic contaminants with the nitrogen-doped porous biochars co-pyrolyzed from macroalgae and oyster shell, providing a potential green resource utilization of aquatic wastes for environmental remediation.

## Highlights

- Nitrogen-doped porous biochars (NPBs) were derived from natural wastes.
- Oyster shell enhanced the micropore and mesopore structures of NPBs.
- Physical sorption dominated atrazine sorption onto the NPBs.

**Keywords** Co-pyrolysis, Macroalgae, Oyster shell, Atrazine, Sorption

Handling editor: Wenfu Chen.

[†]Liying Song and Hu Cheng contributed equally to this work.

*Correspondence:
Yang Song
ysong@issas.ac.cn
Full list of author information is available at the end of the article

**Graphical Abstract**

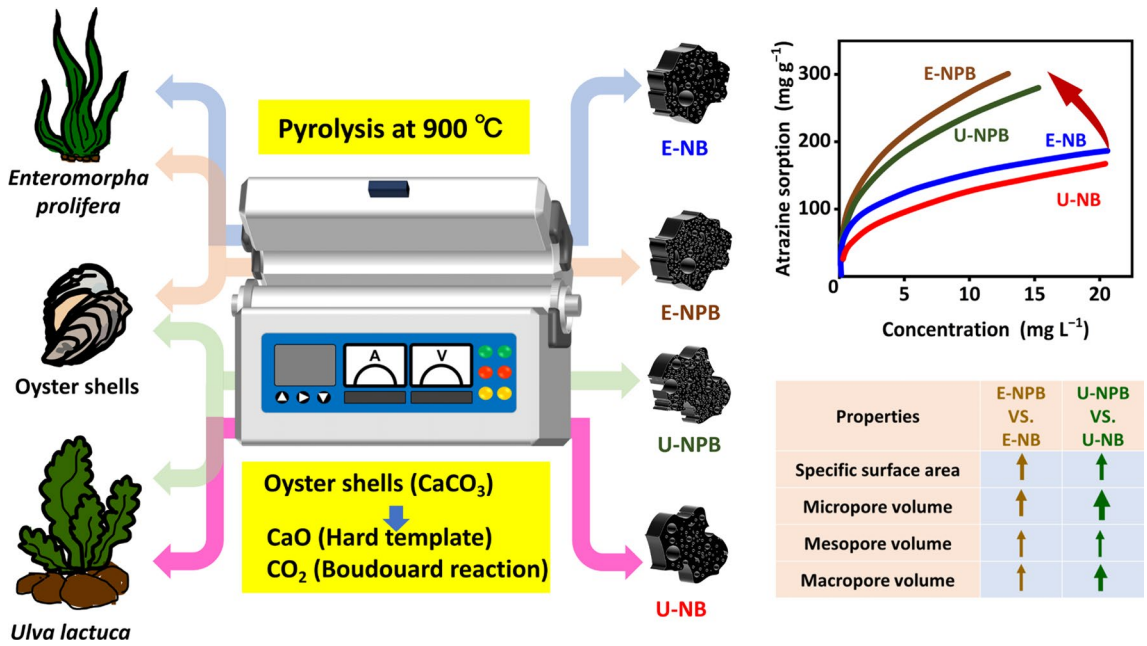


## 1 Introduction

Herbicides, despite playing an important role in global agricultural production, may cause environmental contamination due to their common overapplication and toxicity (Rumschlag et al. 2019). Atrazine, namely 2-chloro-4-ethylamino-6-isopropylamino-1,3,5-triazine, is a typical representative of organic triazine herbicides, widely used in agriculture (Jiang et al. 2022). It was reported that only 10–30% of atrazine is sorbed by grass when applied, and the vast majority enters water or soil via irrigation or precipitation (Cao et al. 2023b). The herbicide shows a long-term stability in natural water environment, owing to its persistence (Liang et al. 2022). Atrazine could be detected in up to 43% of the world's surface freshwaters, including rivers, reservoirs, streams, lakes, and ponds, with the average concentration ranging from 0.0012 to 4.8 μg $L^{-1}$ (de Araujo et al. 2022). Atrazine has potential adverse effects on aquatic organisms, being mutagenic and genotoxic, interfering with cell division and causing endocrine disruption in aquatic animals, as well as affecting photosynthesis, enzymatic reactions and growth of aquatic plants (Rostami et al. 2021). Due to endocrine disrupting activity, atrazine poses potential adverse effects on natural biota and humans, so its removal from water is of great significance in terms of minimizing the health and environmental risks.

Various remediation strategies, including biological, chemical, and physical methods, have been used to limit the negative impact of atrazine on water environment (Rostami et al. 2021). Among them, sorption is one of the highly recommended methods due to its great removal efficiency, simplicity in implementation, low costs, and generating no harmful byproducts (Yao et al. 2019). Previous studies have shown that biochar (Wang et al. 2020b), bentonite clay (Duran et al. 2019), and zeolite (Lee et al. 2020) could effectively sorb and remove atrazine from water. Among these sorbents, biochar is of great concern due to its large specific surface area (SSA), well-developed porous structures and abundance in surface functional groups (Ji et al. 2021). A good example of such an effective sorbent could be a corn stover biochar with atrazine sorption capacity reaching up to 95.93 mg $g^{-1}$ (Wang et al. 2020b).

In situ or post-treatment modifications of biochar were many times proven to be highly effective in creating advanced materials for various environmental applications, including the water treatment (Wang et al. 2020b). Recently, a new kind of biochar derived from marine algae, the species responsible for eutrophication in the oceans, has been developed (Lee et al. 2020). Not all marine algae produce similar biochar. The contents of lipids, proteins and carbohydrates in the algae biomass ranged from 0.9–30.0%, 8.4–65.2% and 10.7–56.9%,

respectively (Wang et al. 2024). During the pyrolysis process, the carbonization intensity and reaction intensity of different components vary, resulting in different pore structures and elemental compositions (Ansah et al. 2018). The inner structure of various marine algae species was different, leading to differences in the number and shape of pores. The amounts of metal salts in various marine algae species also differed, which affected the co-pyrolysis process. Only suitable marine algae species can be transformed into expected biochars. Due to the high content of proteins in macroalgae, it was possible to directly prepare nitrogen (N)-doped biochars (NBs). NBs generally have stronger electron-donor–acceptor interaction (EDA interaction), larger SSA and richer pore structure, as well as more N-functional groups, resulting in greater sorption ability than other biochars without N doping (Gao et al. 2022). For example, *Saccharina japonica* macroalgae-derived biochar exhibits a great sorption efficiency for cationic dye (Boakye et al. 2019). However, the macroalgae biomass in general, lacks lignin, which, in turn, limits the pore structure and SSA of biochars produced from this input material (Poo et al. 2018). Therefore, to enhance the surface area of the macroalgae derived biochars pore-forming agents are commonly used to prepare N-doped porous biochars (NPBs). Most of the conventional pore-forming reagents are corrosive (Tan et al. 2017), and thus their environmental application is limited. Hence, there is a growing demand for a new, cost-effective and environment-friendly pore-forming agent for macroalgae biochars production. Recently, calcium carbonate ($CaCO_3$) has been proposed to activate biochars (Li et al. 2020). At pyrolysis temperatures between 700 and 900 °C, $CaCO_3$ decomposes into calcium oxide (CaO) and carbon dioxide ($CO_2$). CaO may act as a hard template for mesopore creation and $CO_2$ is capable of developing micropores through Boudouard reaction with biochar. The above-mentioned reaction is the dissociation of $CO_2$ on the carbon surface to form carbon monoxide (CO), which is subsequently desorbed from the surface of biochar resulting in the formation of the porous structures (Sajjadi et al. 2019). Analogous to the pure $CaCO_3$, the use of biowastes with high $CaCO_3$ content may also play a similar activation role in biochar production. Based on this, oyster shell, containing up to 96% of $CaCO_3$ per dry mass (Ok et al. 2011), may be a promising activation agent. It was found that the high SSA and well-developed pore structures of the biochar co-pyrolyzed from cotton/polyester waste and oyster shell contribute to its high sorption efficiency for tetracycline, relative to that pyrolyzed without oyster shell (Gu et al. 2021). Moreover, compared to pure $CaCO_3$, the use of oyster shell of solid waste would greatly reduce the cost of biochar production and would be an environment-friendly strategy for recycling and utilizing of natural wastes.

The objective of this study was to prepare efficient sorbents for the removal of atrazine from water bodies using natural wastes. It is hypothesized that the high contents of $CaCO_3$ in oyster shell could activate the macroalgae NBs via enhancing the pore structures, especially the micropores and mesopores, and this could be achieved by one step co-pyrosis process. Therefore, two main types of macroalgae, *Enteromorpha prolifera* and *Ulva lactuca*, which have higher content of carbohydrates and proteins than other macroalgae (Lee et al. 2020), were selected and co-pyrolyzed with oyster shell, *Ostreidae*, to obtain NPBs. Batch sorption experiments were conducted to elucidate the sorption kinetics, isotherms, and potential mechanism of atrazine interaction with the NPBs. To the best of our knowledge, this is the first study to use oyster shell as a pore-forming agent to activate macroalgae-derived biochar for the removal of atrazine from water.

## 2 Materials and methods

### 2.1 Materials and reagents

Macroalgae of *Enteromorpha prolifera* and *Ulva lactuca*, and oyster shell of *Ostreidae* were obtained from the Xiangshan Harbour (29° 28′–29° 30′ N, 121° 40′–121° 46′ E), Zhejiang, China. Hydrochloric acid (HCl, guaranteed reagent) was obtained from Sinopharm Chemical Reagent Co., Ltd. (Beijing, China). Atrazine (≥ 99%) was purchased from Dr. Ehrenstorfer (Augsburg, Germany) and methanol (HPLC grade) was obtained from Accustandard Inc. (New Haven, CT, USA). Ultrapure water (Millipore, Synergy UV) was used in all of the experiments.

### 2.2 Synthesis of the NBs and NPBs

*Enteromorpha prolifera*, *Ulva lactuca,* and oyster shell were washed with ultrapure water and dried in the oven, then ground and passed through a 50-mesh sieve. Afterward, the dried *Enteromorpha prolifera* powder was placed in a tube muffle furnace to produce *Enteromorpha prolifera* derived biochar (E-NB). The temperature was set to 900 ℃ at 3 ℃ $min^{-1}$, and kept for 2 h. Nitrogen ($N_2$) was used at a rate of 200 mL $min^{-1}$ to ensure anoxic conditions during the pyrolysis process. After that, the tube muffle furnace was cooled to room temperature. Then the black carbonaceous product in the tube muffle furnace was collected, ground, and washed with HCl solution until no $Ca^{2+}$ was detected. It was subsequently washed in the ultra-pure water and dried in a conventional oven to finally obtain E-NB. The production of *Ulva lactuca* derived NB (U-NB) followed the analogous procedure as described above.

To obtain the NPBs, biomass of *Enteromorpha prolifera* or *Ulva lactuca* was mixed with oyster shell in a ratio of 2:1

(*w:w*) and placed in a tube muffle furnace (Shi et al. 2020). The pyrolysis process and conditions were the same as those mentioned above. Thus, the *Enteromorpha prolifera* and oyster shell co-pyrolyzed carbonaceous (E-NPB) and the *Ulva lactuca* and oyster shell co-pyrolyzed carbonaceous (U-NPB) were obtained, respectively.

### 2.3 Characterization of NBs and NPBs

The elemental contents of C, H, O, and N in NBs and NPBs were determined using an elemental analyzer (UNICUBE, Germany). Scanning electron microscope (SEM; Regulus 8100, Japan) and transmission electron microscope (TEM; FEI Tecnai G2 F30) were used to characterize the surface morphology and porosity of NBs and NPBs. The pore structures of NBs and NPBs were analyzed applying $N_2$ sorption/desorption isotherm (Micromeritics ASAP 2020 spectrophotometer, USA), Brunauer–Emmett–Teller (BET) model, and Barret-Joyner-Halenda (BJH) model. The crystal structure and graphitization degree of NBs and NPBs were observed using X-ray diffraction (XRD; Smart Lab X-ray diffractometer, Rigaku, Japan) and Raman spectroscopy (in Via-Reflex, Renishaw, England). Changes in the surface elemental composition, C-valence bond state, and surface functional groups of NBs and NPBs were studied by X-ray photoelectron spectroscopy (XPS; Escalab 250xi, Thermo Scientific, USA) and Fourier transform infrared spectroscopy (FTIR; Nicolet iS10, Thermo Fisher Nicolet., USA).

### 2.4 Batch sorption experiments

The sorption kinetics and isotherms studies of atrazine by NBs and NPBs were conducted. Briefly, ultrapure water was used as background solution in which $NaN_3$ (200 mg $L^{-1}$) was added as a biocide. 1 mg of E-NB, or U-NB, or E-NPB, or U-NPB, was added to 20 mL of water, placed in a brown bottle that was wrapped in tinfoil to avoid photolysis. Then the bottles were placed in a rotary shaker (WH-962) set to 50 revolution $min^{-1}$ at 25 ℃. In the sorption kinetics experiment, the initial concentration of atrazine was 5 mg $L^{-1}$, and time intervals were set to: 0, 0.5, 1, 2, 4, 8, 12, 24, 48, 72, 96 h. The sorption isotherm experiments were conducted with the following concentrations of atrazine: 1.5, 3, 5, 10, 15, 20, 30 mg $L^{-1}$, and 72 h of equilibration. All the batch sorption experiments were conducted in triplicate. After shaking, the mixtures were centrifuged at 10,000 revolution $min^{-1}$ for 3 min, and the supernatants were analyzed by high-performance liquid chromatography (HPLC, Agilent Technologies 1260 Infinity II). The sorption capacity ($Q$) was calculated as:

$$Q = (C_0 - C)V/m$$

in which, $C_0$ (mg $L^{-1}$) is the original pollutant concentration, $C$ (mg $L^{-1}$) represents the residual concentration at the time of sampling, and $V/m$ is related to the reaction volume (L)/ sorbent material dosage (g).

The NBs and NPBs before and after the sorption experiments were also collected and analyzed by FTIR.

### 2.5 Recycling and recovery experiment

In order to further investigate the reuse potential of NBs and NPBs and the recovery of atrazine, we developed a method to study the sorption capacity and recovery of atrazine by re-pyrolysis. At the end of the sorption experiments, the carbonaceous substance was separated using a pumping device, and the collected carbonaceous substance containing atrazine was dried and then placed in a muffle furnace. The heating rate was set at 3 ℃ $min^{-1}$. The final temperature was set at 900 °C and maintained for 2 h. After that, the tube muffle furnace was cooled to room temperature, and the NBs and NPBs were removed from the muffle furnace and used for the next cycle of sorption experiments.

### 2.6 Analysis of atrazine

The concentration of atrazine in the solution was determined by HPLC using a $C_{18}$ column (4.6 mm × 250 mm, 5 μm) and an ultraviolet detector at the wavelength of 220 nm. The mobile phase was methanol and ultra-pure water in the ratio of 6: 4 (*v*: *v*). The column temperature was 35 ℃, with the flow rate of 1 mL $min^{-1}$ and the injection volume of 20 μL.

### 2.7 Quality control and data analysis

Control experiments with different initial atrazine concentrations and without sorbents were conducted to ensure that there was no sorption of the herbicide on the vial walls. None of the E-NB, U-NB, E-NPB, and U-NPB contained atrazine. The recoveries of the herbicide in the sorption experiments ranged from 79.14 to 98.53%, and the relative standard deviation was lower than 5.94%. The origin 2022b (version 8.5) and sigmaplot (version 15) were used to analyze and process the experimental data. Four kinetic models including pseudo-first-order, pseudo-second-order, elovich model, and two-compartment (TC) model, and three isotherm models including Langmuir, Freundlich, and Temkin were used for data fitting. The detailed parameters are shown in Table S1.

## 3 Results and discussion

### 3.1 Characterization of NBs and NPBs

The elemental compositions of NBs and NPBs are presented in Table S2. In NPBs, the abundance of C (78.91%, 80.12%) increased, while the shares of O (9.67%, 9.03%) and S (1.81%, 1.91%) decreased, compared to NBs (C, 72.49%, 71.48%; O, 13.99%, 15.78%; S, 5.21%, 5.51%). The changes in C content could be attributed to the fact

that $CO_2$ generated from the decomposition of $CaCO_3$ promoted the carbonization reaction by facilitating the deoxygenation and dehydrogenation processes to generate carbon-rich biochar (Yi et al. 2022). The N contents in NBs and NPBs were similar and higher than in other biochars derived from corn stover and maple (Choudhury and Lansing 2020). This is consistent with the other studies, supporting high N content in algal biochars (Ji et al. 2021; Wen et al. 2022). Furthermore, the ash content was 4.30%, 2.30%, 5.50%, and 4.71% for E-NB, U-NB, E-NPB, and U-NPB, respectively. The ash content increased after the activation of oyster shell. Certain minerals from oyster shell were preserved in the biochar matrix. The H/C ratios decreased during co-pyrolysis, indicating the increased aromaticity of NPBs, which is typically observed in high-temperature biochars (Hong et al. 2019). Meanwhile, O/C and (N + O)/C ratios were also reduced, indicating the decrease in polar functional groups and increase in hydrophobicity of NPBs.

Scanning electron microscopy revealed that the surfaces of NBs were uneven and wrinkled with a smooth surface (Fig. S1). Meanwhile, the NPBs were more abundant in rough structures than NBs. There was obvious void structure in E-NPB, providing large SSA for sorption. In addition, the TEM images demonstrated that NPBs contained more graphene stripes than NBs. The $N_2$ sorption–desorption isotherm provided a further detailed characteristics of the changes in SSA and pore size distribution of NBs and NPBs (Fig. 1). Briefly, the co-pyrolysis of macroalgae and oyster shell increased the SSA of the NPBs. The SSA of E-NPB (1501.80 $m^2$ $g^{-1}$) was 2.82 times higher than that of E-NB (532.02 $m^2$ $g^{-1}$), and the SSA of U-NPB (1067.18 $m^2$ $g^{-1}$) was 2.66 times higher than that of U-NB (400.47 $m^2$ $g^{-1}$). The pore volumes of NPBs were also increased relative to those of NBs. The pore volume of E-NPB was 2.02 times higher than that of E-NB, and the pore volume of U-NPB was 1.88 times higher than that of the U-NB. The pore size distribution was basically below 10 nm, and most distributed around 1.30 nm and 7.50 nm (Fig. 1(b)). The average pore size was 4.83 nm, 6.76 nm, 4.28 nm, and 5.34 nm for E-NB, U-NB, E-NPB, and U-NPB, respectively, indicating that the co-pyrolysis with oyster shell decreased the average pore size in NPBs. Furthermore, the micropore volume and mesopore volume in E-NPB were 9.14 and 1.88 times higher than those of E-NB, respectively. While the analogous parameters for U-NPB were 1696.73 and 1.69 times higher than those for U-NB, respectively. This result indicated that the co-pyrolysis of oyster shell with macroalgae mainly increased the micropores and mesopores structures of the NPBs, thus increasing their SSA.

The crystal structures of NBs and NPBs (Fig. S2(a)), revealed diffraction peaks at 20–30° and 40–50° for E-NB, U-NB, E-NPB, and U-NPB, which were attributed to the corresponding reflections of the graphite structure (Cao et al. 2012). The 15° peaks for E-NPB and U-NPB indicate the ash content from oyster shell, which is consistent with the element analysis results. Raman spectroscopy analysis was conducted to further confirm the graphitized degree of NBs and NPBs (Fig. S2(b)). Two different characteristic peaks appeared at 1350 $cm^{-1}$ (D peak) and 1590 $cm^{-1}$ (G peak) for biochar, which represented a degree of edge defects and ordered graphite

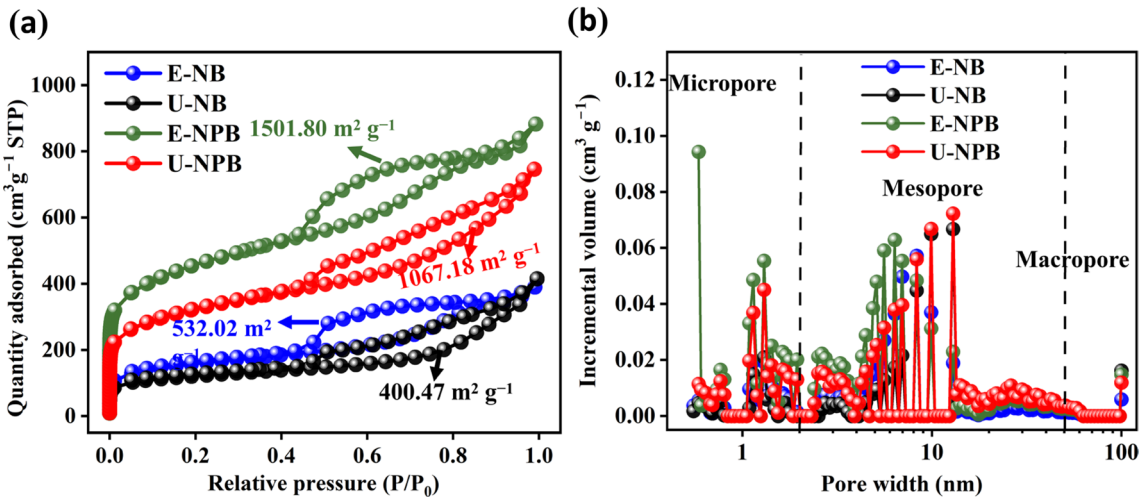


**Fig. 1** Nitrogen adsorption–desorption isotherms (**a**) and pore size distributions (**b**) of *Enteromorpha prolifera* derived nitrogen-doped biochar (E-NB), *Ulva lactuca* derived nitrogen-doped biochar (U-NB), *Enteromorpha prolifera* and oyster shell co-pyrolyzed nitrogen-doped porous biochar (E-NPB), and *Ulva lactuca* and oyster shell co-pyrolyzed nitrogen-doped porous biochar (U-NPB)

degree of carbon atoms, respectively. Compared to NBs, the $I_D$ (the intensity of the D band) / $I_G$ (the intensity of the G band) values of NPBs decreased, indicating that the process of co-pyrolysis is related to the increase of graphite degree, which is consistent with the TEM analysis results.

Minor changes in the surface functional groups of NBs and NPBs were observed in the FTIR (Fig. S3). The transmittance spectra illustrated that NBs and NPBs contained peaks characteristic for stretching and bending vibrations of −OH (3436−3442 $cm^{-1}$), $-CH_2$ or $-CH_3$ (2930 $cm^{-1}$), C=O or C=C (1617−1624 $cm^{-1}$), C−O−C (1096−1101 $cm^{-1}$) and −CH (802−803 $cm^{-1}$) (Zhao et al. 2022). Notably, the N−H stretching vibrational signal was observed at 1460 $cm^{-1}$, which was due to the presence of relatively high abundance of nitrogen in the macroalgae itself (Yuan et al. 2023). The functional group peaks exhibited slight changes after co-pyrolysis, which showed an increase in the peak intensity of –OH at 3437 $cm^{-1}$ for E-NPB and U-NPB, as well as a decrease in the C−O−C peak intensity at 1097 $cm^{-1}$, indicating that the co-pyrolysis protects –OH and destroys C−O−C.

The XPS analysis of NBs and NPBs further evidenced the primary elements in the surface, valence bond, and content (Fig. S4). The primary elements in NBs and NPBs were C, O, and N, in line with other algal biochars' composition (Nguyen et al. 2022). The acid washing effectively removed CaO, resulting in clean surface composition of NPBs. In NBs and NPBs, the C peak can be divided into five types: C=C, C–C, C–O, C=O, and O–C=O (Yao et al. 2019). The influence of oyster shell on the C structure of the NPBs was relatively small, with a slight increase in C=C and C=O in E-NPB and C=C and O–C=O in U-NPB, which could promote sorption through π-π interaction and hydrogen bonding. The high-resolution N 1s spectrum contained four peaks, including pyridinic-N (N-6), pyrrolic-N (N-5), graphitic-N (N-Q) and oxidized pyridinic-N (N-X). Interestingly, N-5 content dominated the N composition in NPBs, thus increasing the potential formation of hydrogen bonds between pollutants and biochar (Cheng et al. 2022).

### 3.2 Sorption kinetics of atrazine to NBs and NPBs

The sorption kinetics of atrazine on NBs and NPBs and the model fitting parameters are presented in Fig. 2 and Table 1, respectively. As might be expected, the sorption process in the first 30 min was rapid, followed by the decrease of sorption rate. The sorption process of atrazine on E-NB, U-NB, E-NPB, and U-NPB reached equilibrium within 4 h, 24 h, 3 h, and 8 h, respectively (Fig. 2(a)), indicating that this time was reduced after co-pyrolysis. This might be due to the superior pore structure and higher graphite degree of NPBs compared to NBs, especially for U-NPB. The pseudo-second-order model with the higher $R^2$ and lower *SEE* values described the atrazine sorption on NBs and NPBs better than the pseudo-first-order model, which suggests that chemisorption would be a rate-controlling step (Tao et al. 2020). The $k_2$ values of E-NPB and U-NPB were higher than these of E-NB and U-NB, evidencing that the former exhibited better sorption strength and affinity for atrazine.

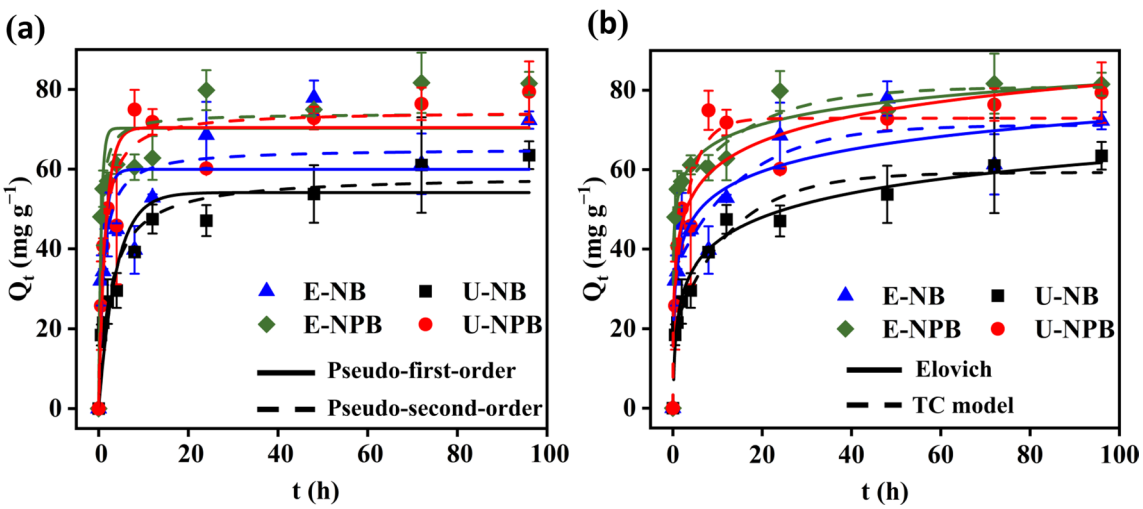


**Fig. 2** Sorption kinetics of atrazine onto *Enteromorpha prolifera* derived nitrogen-doped biochar (E-NB), *Ulva lactuca* derived nitrogen-doped biochar (U-NB), *Enteromorpha prolifera* and oyster shell co-pyrolyzed nitrogen-doped porous biochar (E-NPB), and *Ulva lactuca* and oyster shell co-pyrolyzed nitrogen-doped porous biochar (U-NPB). Pseudo-first-order model (solid curves) and Pseudo-second-order model (dashed curves) (**a**); Elovich model (solid curves) and TC model (dashed curves) (**b**). $Q_t$ (mg $g^{-1}$) is the solid concentration of atrazine adsorbed at the contact time t (h)

**Table 1** Kinetic parameters of atrazine onto nitrogen-doped biochars (NBs) and nitrogen-doped porous biochars (NPBs)

| | Pseudo-first-order | | | | Pseudo-second-order | | | | Elovich | | | | TC model | | | | | | |
|---|---|---|---|---|---|---|---|---|---|---|---|---|---|---|---|---|---|---|---|
| | $k_1$ | $Q_t$ | $R^2$ | *SEE* | $k_2$ | $Q_t$ | $R^2$ | *SEE* | $\alpha$ | $\beta$ | $R^2$ | *SEE* | $Q_t$ | $F_{fast}$ | $F_{slow}$ | $k_{fast}$ | $k_{slow}$ | $R^2$ | *SEE* |
| E-NB | 0.9 | 59.94 | 0.705 | 12.07 | 0.016 | 65.15 | 0.807 | 9.75 | 672.16 | 0.12 | 0.898 | 7.52 | 71.21 | 0.53 | 0.47 | 0.07 | 201.26 | 0.88 | 16.23 |
| U-NB | 0.26 | 54.12 | 0.844 | 7.79 | 0.007 | 58.44 | 0.923 | 5.47 | 103.30 | 0.11 | 0.983 | 2.73 | 59.27 | 0.32 | 0.68 | 54,042.67 | 0.08 | 0.955 | 14.51 |
| E-NPB | 1.81 | 70.26 | 0.837 | 9.33 | 0.036 | 73.96 | 0.903 | 7.19 | 22,593.80 | 0.16 | 0.974 | 3.92 | 80.81 | 0.64 | 0.36 | 8,044,328.07 | 0.06 | 0.965 | 12.52 |
| U-NPB | 0.65 | 70.43 | 0.873 | 8.93 | 0.013 | 74.57 | 0.919 | 7.13 | 752.53 | 0.11 | 0.901 | 8.37 | 72.93 | 0.33 | 0.67 | 246,895.47 | 0.27 | 0.877 | 13.03 |

*Enteromorpha prolifera* derived nitrogen-doped biochar (E-NB), *Ulva lactuca* derived nitrogen-doped biochar (U-NB), *Enteromorpha prolifera* and oyster shell co-pyrolyzed nitrogen-doped porous biochar (E-NPB), and *Ulva lactuca* and oyster shell co-pyrolyzed nitrogen-doped porous biochar (U-NPB). $Q_t$ is the sorption amount at time t and sorption equilibrium respectively (mg $g^{-1}$); $k_1$ and $k_2$ are pseudo-first-order and pseudo-second-order rate constants, respectively, and the units are ($h^{-1}$) and (g $mg^{-1}$ $h^{-1}$), respectively. *SEE* is standard error of estimate. $\alpha$ is the initial sorption coefficient (mg (g $h^{-1}$)) and $\beta$ is the desorption rate constant (g $mg^{-1}$). $F_{fast}$ represents the proportion of components in the rapid adsorption reaction, while $F_{slow}$ represents the proportion of components in the slow adsorption reaction. $k_{fast}$ and $k_{slow}$ are the rate constants ($h^{-1}$) of the fast and slow reactions, respectively

The sorption process was also described by the elovich model which is applied to chemisorption phenomena occurring on non-homogeneous sorbents. The model fitted the data well with $R^2$ values within the range of 0.90–0.98 and *SEE* values within 2.73–8.37 (Fig. 2(b)), which suggests a substantial role of chemisorption mechanism in interactions of atrazine with the studied biochars (Zanli et al. 2022). In addition, the TC model was used to further investigate the sorption process of atrazine (Fig. 2(b)). Within the time of about 24 h, during the fast sorption step, E-NB, U-NB, E-NPB, and U-NPB reached 89.48%, 89.37%, 91.82%, and 99.90% of the sorption equilibrium, respectively. The slow step accounted for the rest of the sorption share within the next 72 h. This may be related to the surface properties of NBs and NPBs, which have higher SSA and massive pore structures (Fig. 1), actively involved in atrazine sorption during the first 24 h of its contact with the sorbents.

### 3.3 Sorption isotherms of atrazine onto NBs and NPBs

Freundlich, Langmuir, and Temkin models were used to fit the sorption isotherms of atrazine on NBs and NPBs (Fig. 3 and Table 2). Generally, the Freundlich model fitted the sorption isotherms of NBs and NPBs better than the Langmuir model (Table 2), indicating that the sorption of atrazine to NBs and NPBs occurs via multilayers (Liu et al. 2017). The multilayer sorption of atrazine to woodchips and barks biochar (Zheng et al. 2010), peanut-shell biochar (Wang et al. 2020a) and corn stover with sawdust powder biochar (Gao et al. 2019) was also reported. The $k_f$ values of E-NPB and U-NPB were higher than those of E-NB and U-NB, indicating that E-NPB and U-NPB exhibit strong sorption intensity for atrazine. The Temkin model was used to evaluate whether the sorption of atrazine on NBs and NPBs was of physical or chemical nature (Fig. 3(b) and Table 2). The adsorption energy ($b$) of typical physical sorption process is less than < −40

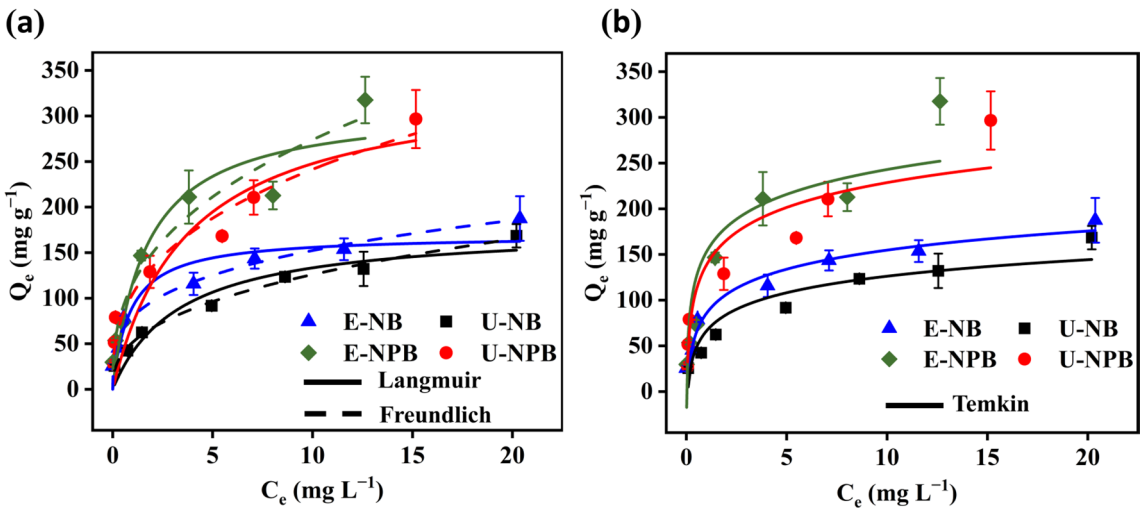


**Fig. 3** Sorption isotherms of atrazine onto *Enteromorpha prolifera* derived nitrogen-doped biochar (E-NB), *Ulva lactuca* derived nitrogen-doped biochar (U-NB), *Enteromorpha prolifera* and oyster shell co-pyrolyzed nitrogen-doped porous biochar (E-NPB), and *Ulva lactuca* and oyster shell co-pyrolyzed nitrogen-doped porous biochar (U-NPB). **a** Langmuir model (solid lines), Freundlich model (dashed lines); **b** Temkin model. $Q_e$ (mg g$^{-1}$) is the amount of atrazine adsorbed to the biochars; $C_e$ (mg L$^{-1}$) is the equilibrium concentration in solution

**Table 2** Isotherm parameters of atrazine onto nitrogen-doped biochars (NBs) and nitrogen-doped porous biochars (NPBs)

| | Langmuir | | | | Freundlich | | | | Temkin | | | |
|---|---|---|---|---|---|---|---|---|---|---|---|---|
| | $k_l$ | $Q_{max}$ | $R^2$ | *SEE* | $k_f$ | $n$ | $R^2$ | *SEE* | $a$ | $b$ | $R^2$ | *SEE* |
| E-NB | 1.15 | 169.34 | 0.884 | 20.29 | 79.36 | 0.28 | 0.946 | 13.81 | 17.05 | 0.082 | 0.940 | 15.50 |
| U-NB | 0.30 | 178.07 | 0.915 | 15.18 | 51.52 | 0.39 | 0.991 | 4.85 | 12.66 | 0.095 | 0.875 | 18.40 |
| E-NPB | 0.60 | 312.06 | 0.901 | 32.91 | 115.55 | 0.37 | 0.948 | 23.81 | 49.09 | 0.063 | 0.803 | 46.37 |
| U-NPB | 0.27 | 340.52 | 0.804 | 42.3 | 104.65 | 0.36 | 0.958 | 19.63 | 34.07 | 0.063 | 0.876 | 33.64 |

*Enteromorpha prolifera* derived nitrogen-doped biochar (E-NB), *Ulva lactuca* derived nitrogen-doped biochar (U-NB), *Enteromorpha prolifera* and oyster shell co-pyrolyzed nitrogen-doped porous biochar (E-NPB), and *Ulva lactuca* and oyster shell co-pyrolyzed nitrogen-doped porous biochar (U-NPB). $Q_{max}$ is the maximum sorption capacity (mg g$^{-1}$); $k_l$ is the Freundlich constant (L mg$^{-1}$); *SEE* is standard error of estimate. $k_f$ is the Freundlich constant ((mg g$^{-1}$) (mg L$^{-1}$)$^{-n}$); $n$ is the sorption affinity constant; $a$ and $b$ are Temkin constants (L g$^{-1}$, kJ mol$^{-1}$)

kJ $mol^{-1}$, and the bonding energy of typical chemical interaction is in the range of 8–16 kJ $mol^{-1}$ (Hu et al. 2011). In this study, the values of *b* for E-NB (0.082 kJ $mol^{-1}$), U-NB (0.095 kJ $mol^{-1}$), E-NPB (0.063 kJ $mol^{-1}$) and U-NPB (0.063 kJ $mol^{-1}$) indicated that the sorption of atrazine on NBs and NPBs involved both physical and chemical sorption, but was mainly governed by physical sorption (Kiran and Kaushik 2008). The *b* exhibited decreasing trend when comparing NBs and NPBs (Table 2). According to the model assumptions, this may suggest the increase in surface coverage with atrazine for NPBs (Franus et al. 2019).

### 3.4 Sorption mechanisms of atrazine to NBs and NPBs

As it was shown by the isotherms fitting, the sorption of atrazine to NBs was a process dominated by physical interactions, facilitated by their porous structure and relatively high SSA. The sorption of atrazine to E-NB was faster than that to U-NB, whilst the sorption capacity of atrazine for U-NB was greater than that for E-NB. These observations can be explained by the fact that U-NB was relatively abundant in C=C moieties, which might also enhance chemical interactions with atrazine. Based on the FTIR spectra (Fig. S3) it could be noticed that during the sorption of atrazine on NBs, such as E-NB, the main shifts were related to −OH, C=O or C=C, and C−O−C groups (3441 → 3432 $cm^{-1}$, 1619 → 1576 $cm^{-1}$, and 1101 → 1099 $cm^{-1}$). That could be attributed to the functional group complexation and hydrogen bonding in the sorption process. In addition, only C−H was shifted in the case of the herbicide sorption to by U-NB. Thus, it appeared that the sorption of atrazine by NBs was closely related to chemical functionalities of biochars, such as the presence of C=C groups and N-doping. It was found that the nitrogen atoms added reduced the electron density on the surface of biochar and enhanced its ability to accept electrons. Furthermore, atrazine is considered an electron donor due to its electron-rich nature (Yang et al. 2017). Thus, the NBs were able to interact with triazine heterocycles or nitrogen lone pairs of electrons in atrazine for π-π EDA or *p*-π EDA, respectively (Cao et al. 2023a). In the study, the equilibrium pH values for sorption of atrazine by NBs and NPBs were centered at 6–7. The dominate species of atrazine represented the positive charges at pH range of 5.5–7 because of the protonation according to Yan et al.( 2022). Therefore, under the experimental conditions in this study, electrostatic interaction had effect on the sorption of atrazine on NBs and NPBs.

After co-pyrolysis with oyster shell, the sorption capacity of NPBs for atrazine significantly increased, E-PNB increased by more than 1.84 times compared to E-NB, and U-PNB increased by more than 1.91 times compared to U-NB ($p < 0.05$), which could be attributed to the enhanced SSA, pore volume, C content and other surface properties of NPBs. Firstly, the increase in SSA and pore structures of NPBs was crucial for the overall elevation of the sorption capacity of atrazine, especially micropores and mesopores. Due to the decomposition of $CaCO_3$ from oyster shell into $CO_2$ and CaO, the $CO_2$ gas flux eroded the material to promote the formation of micropores below 0.7 nm (Li et al. 2023), the CaO formed 13–23 nm mesopores by embedding into the carbon body after acid washing (Islam et al. 2014), thus providing more sorption sites and storage space and enhancing the mass transfer process between atrazine and NPBs. In order to better assess the effect of different pore structures on the sorption of atrazine on carbon samples, the correlations between the maximum sorption capacity ($Q_{max}$) and pores were analyzed. The relationships between $Q_{max}$ and micropore or mesopore volume were higher than for $Q_{max}$ and macropore volume (Fig. 4), indicating that the sorption of atrazine was favored by the abundant sorption sites in micropores and mesopores (0.96 nm × 0.84 nm × 0.3 nm) on NPBs (Cheng et al. 2022). Therefore, the pore filling to micropores and mesopores played the most important role in the sorption of atrazine to NBs and NPBs. Therefore, we may co-pyrolyze with potassium and calcium salts to increase the micropore and mesopore structures to further improve the sorption of atrazine in the future (Yan et al. 2022; Sajjadi et al. 2019).

Secondly, combined variations in the polarity, aromaticity, and hydrophobicity of NPBs prompted differences in sorption capacity between NBs and NPBs. In this study, it was found that the aromaticity, as indicated by H/C, increased with the co-pyrolysis (Table S2). Atrazine, as a hydrophobic organic contaminant, would be preferentially sorbed by carbonaceous sorbents via π-π EDA and hydrogen bonding. The high degree of graphitization of NPBs also indicated the presence of a large number of electron-deficient aromatic rings (Fig. S2(b)), which are π-electron acceptors, while atrazine acts as an electron donor, rich in π-electrons, further favoring the sorption (Fig. 5). Based on the FTIR analysis, it could be noticed that there were significant shifts in C=C or C=O bands and the intensity change in −CH of E-NPB as well as in −OH of U-NPB due to atrazine sorption indicates relatively strong π-π EDA and hydrogen bonding interactions (Yao et al. 2019). Meanwhile, the O/C and (O + N)/C values demonstrated that the NPBs had less polar functional groups and stronger hydrophobicity than NBs (Table S2), which supports the presence of relatively strong hydrogen bonding during sorption process. This was additionally evidenced

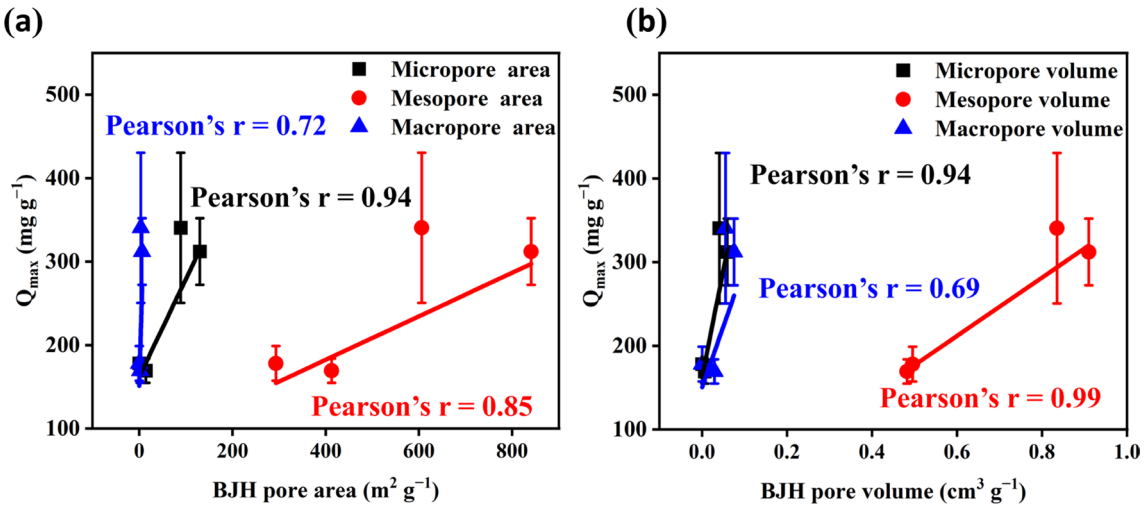


**Fig. 4** Linear correlation between sorption quantities of atrazine onto *Enteromorpha prolifera* derived nitrogen-doped biochar (E-NB), *Ulva lactuca* derived d nitrogen-doped biochar (U-NB), *Enteromorpha prolifera* and oyster shell co-pyrolyzed nitrogen-doped porous biochar (E-NPB), and *Ulva lactuca* and oyster shell co-pyrolyzed nitrogen-doped porous biochar (U-NPB). with the BJH pore area (**a**), BJH pore volume (**b**)

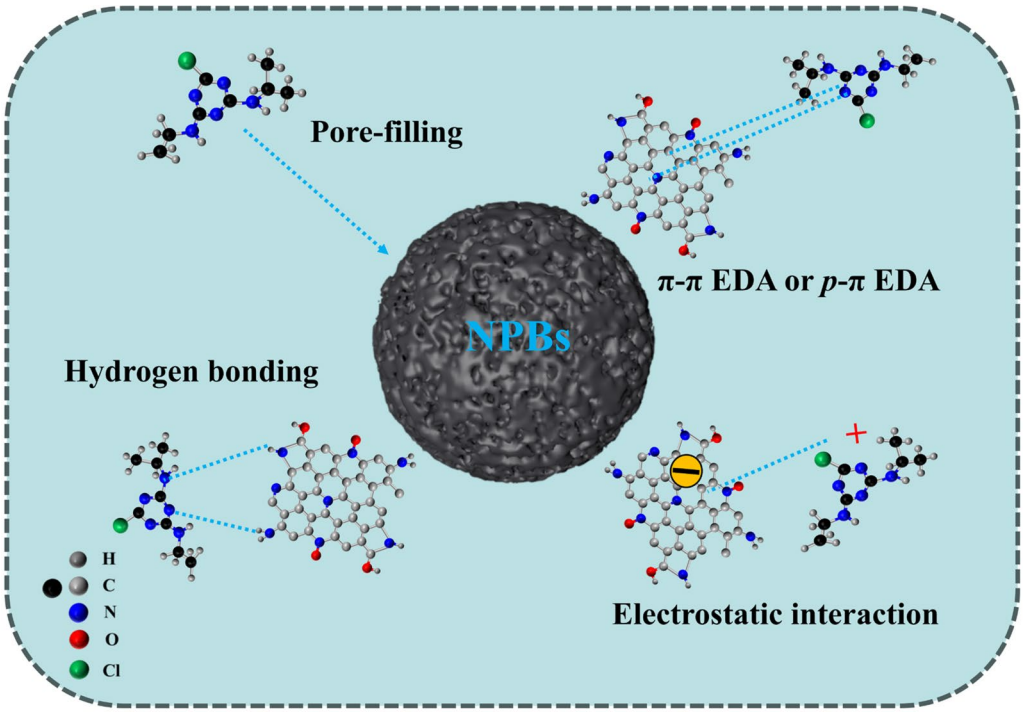


**Fig. 5** Sorption mechanisms of atrazine onto nitrogen-doped porous biochars (NPBs)

by the high-resolution XPS spectra of N1s (Fig. S4(i–l)) showing that the N-5 content on the biochars surface was up to 70% after co-pyrolysis, which enhanced the probability hydrogen bonding interactions during the sorption process (Cheng et al. 2022; Zheng et al. 2010).

### 3.5 Reuse of NBs and NPBs

According to the Langmuir model in different initial concentration conditions, the maximum sorption capacity of atrazine to E-NPB and U-NPB was 312.06 mg g$^{-1}$ and 340.52 mg g$^{-1}$ (Table 2), respectively, which was much higher than that by other reported biochars, including

activated carbon (Gao et al. 2019; Hernandes et al. 2022; Liu et al. 2018; Llado et al. 2015; Netto et al. 2022; Wang et al. 2020a, 2020b) (Table S3). Because the SSA and pore volume of both E-NPB and U-NPB are higher than those reported for biochar (Table S3). Compared with reported N-doped biochar, the NPBs in this study showed much higher sorption capacity than N-doped biochar (Table S4). The NBs and NPBs were also used to sorb atrazine loaded natural lake water, which showed that the sorption capacity of atrazine on NBs and NPBs in natural water was even higher than that in pure laboratory water ($p < 0.05$) (Fig. S5(a)). This is direct evidence that co-pyrolysis of macroalgae and oyster shell is an excellent method for the preparation of highly efficient sorbents. Powdered biochar can be mixed with chitosan and crosslinked to form membranes, beads, solutions, or as a medium to be added to biochar layers/columns for use in filtration systems to treat wastewater (Enaime et al. 2020; Xiang et al. 2020).

To further test the regeneration of the NPBs, a heating treatment for the NPBs after sorption was conducted (Fig. S5(b)). As a result, the sorption capacity of primary pyrolysis of NBs and NPBs towards atrazine was further improved compared to their initial use, and after the twice pyrolysis, the sorption capacity of NPBs for atrazine still reached 246.13 mg $g^{-1}$(E-NPB) and 255.97 mg $g^{-1}$(U-NPB), respectively, which indicated that the NPBs could be cyclically used in treating atrazine contaminated water. By re-pyrolysis, atrazine sorbed on NPBs could be disposed centrally to avoid secondary contamination and the NPBs could be reused. Thus, oyster shell exhibits a great potential for activating biochars during the co-pyrolysis process, which is an economical and environment-friendly way of utilizing aquatic waste as resources in water treatment.

## 4 Conclusions

Oyster shell can be a promising activator for biochar production due to their high $CaCO_3$ content. The co-pyrolysis of macroalgae (*Enteromorpha prolifera* and *Ulva lactuca*) and oyster shell increased the SSA and pore volume of micro/mesopores in NPBs. The SSA of E-NPB and U-NPB reached 1501.80 $m^2$ $g^{-1}$ and 1067.18 $m^2$ $g^{-1}$, and the pore volume reached 1.04 $cm^3$ $g^{-1}$ and 0.93 $cm^3$ $g^{-1}$, respectively. At the same time, the NPBs also exhibited high aromatization and graphitization. As a result, the sorption of atrazine on NPBs was increased compared to NBs, and the sorption of atrazine on E-NPB and U-NPB reached 312.06 mg $g^{-1}$ and 340.52 mg $g^{-1}$, respectively. This study developed a green and low-cost pore-forming method for the preparation of highly efficient porous biochars, providing a new strategy for resources utilization. Therefore, NPBs derived from co-pyrolysis of macroalgae and oyster shell could be used as a strong sorbent for wastewater treatment in factory, especially for high concentration of organic pollutants including herbicides. Additionally, in order to better guide the application of NPBs in various polluted environments, there is a need to evaluate the sorption performance of polluted waters in different real environments in the future. Conducting hundreds or thousands of cycling experiments for performance evaluation of reuse is needed in future studies.

## Supplementary Information

The online version contains supplementary material available at https://doi.org/10.1007/s42773-024-00372-9.

Supplementary Material 1.

**Acknowledgements**
Not applicable.

**Author contributions**
Liying Song: Data curation, Formal analysis, Investigation, Methodology, Writing—original draft. Hu Cheng: Design materials, Data curation, Formal analysis, Investigation. Cuiying Liu: Formal analysis, Investigation. Rongting Ji: Investigation, Methodology. Shi Yao: Formal analysis, Investigation, Methodology. Huihui Cao: Methodology. Yi Li: Investigation. Yongrong Bian: Software. Xin Jiang: Supervision, Writing—review and editing. Irmina Ćwieląg-Piasecka: Writing—review and editing. Yang Song: Conceptualization, Funding acquisition, Supervision, Writing—review and editing.

**Funding**
This study was financially supported by the National Key Research and Development Program of China (2020YFC1807003), the Strategic Priority Research Program of the Sciences (XDA28010501), the Youth Innovation Promotion Association, CAS (2021309), and the National Natural Science Foundation of China (42277303).

**Data availability**
Data will be made available on request.

## Declarations

**Competing interests**
The authors declare that they have no known competing financial interests or personal relationships that could have appeared to influence the work reported in this paper.

**Author details**
[1]State Key Laboratory of Soil and Sustainable Agriculture, Institute of Soil Science, Chinese Academy of Sciences, No. 71 East Beijing Road, Nanjing 210008, People's Republic of China. [2]Co-Innovation Center for the Sustainable Forestry in Southern China, College of Biology and the Environment, Nanjing Forestry University, Nanjing 210037, People's Republic of China. [3]School of Applied Meteorology, Nanjing University of Information Science and Technology, Nanjing 210044, China. [4]Nanjing Institute of Environmental Sciences, Ministry of Ecology and Environment, Nanjing 210042, People's Republic of China. [5]Institute of Soil Science, Plant Nutrition and Environmental Protection, Wroclaw University of Environmental and Life Sciences, Grunwaldzka 53 St., 50-357 Wrocław, Poland.

Received: 11 March 2024 Revised: 23 July 2024 Accepted: 29 July 2024
Published online: 11 September 2024

## References


Ansah E, Wang LJ, Zhang B, Shahbazi A (2018) Catalytic pyrolysis of raw and hydrothermally carbonized chlamydomonas debaryana microalgae for denitrogenation and production of aromatic hydrocarbons. Fuel 228:234–242. https://doi.org/10.1016/j.fuel.2018.04.163

Boakye P, Tran HN, Lee DS, Woo SH (2019) Effect of water washing pretreatment on property and adsorption capacity of macroalgae-derived biochar. J Environ Manage 233:165–174. https://doi.org/10.1016/j.jenvman.2018.12.031

Cao YL, Xiao LF, Sushko ML, Wang W, Schwenzer B, Xiao J, Nie Z, Saraf LV, Yang ZG, Liu J (2012) Sodium ion insertion in hollow carbon nanowires for battery applications. Nano Lett 12:3783–3787. https://doi.org/10.1021/nl3016957

Cao HH, Yao S, Xu L, Bian YR, Jiang X, Cwielag-Piasecka I, Song Y (2023a) Aging of biodegradable-mulch-derived microplastics reduces their sorption capacity of atrazine. Environ Pollut 331:121877. https://doi.org/10.1016/j.envpol.2023.121877

Cao Y, Wang LP, Kang XD, Song JB, Guo HL, Zhang QY (2023b) Insight into atrazine removal by fallen leaf biochar prepared at different pyrolysis temperatures: batch experiments, column adsorption and DFT calculations. Environ Pollut 317:120832. https://doi.org/10.1016/j.envpol.2022.120832

Cheng YZ, Wang BY, Shen JM, Yan PW, Kang J, Wang WQ, Bi LB, Zhu XW, Li YB, Wang SY, Shen LL, Chen ZL (2022) Preparation of novel N-doped biochar and its high adsorption capacity for atrazine based on π-π electron donor-acceptor interaction. J Hazard Mater 432:128757. https://doi.org/10.1016/j.jhazmat.2022.128757

Choudhury A, Lansing S (2020) Biochar addition with Fe impregnation to reduce $H_2S$ production from anaerobic digestion. Bioresour Technol 306:123121. https://doi.org/10.1016/j.biortech.2020.123121

de Araujo EP, Caldas ED, Oliveira-Filho EC (2022) Pesticides in surface freshwater: a critical review. Environ Monit Assess 194:452. https://doi.org/10.1007/s10661-022-10005-y

Duran E, Bueno S, Hermosin MC, Cox L, Gamiz B (2019) Optimizing a low added value bentonite as adsorbent material to remove pesticides from water. Sci Total Environ 672:743–751. https://doi.org/10.1016/j.scitotenv.2019.04.014

Enaime G, Baçaoui A, Yaacoubi A, Lübken M (2020) Biochar for wastewater treatment-conversion technologies and applications. Appl Sci Basel 10:3492. https://doi.org/10.3390/app10103492

Franus M, Bandura L, Madej J (2019) Mono and poly-cationic adsorption of heavy metals using natural glauconite. Minerals 9:470. https://doi.org/10.3390/min9080470

Gao Y, Jiang Z, Li JJ, Xie WL, Jiang Q, Bi MC, Zhang Y (2019) A comparison of the characteristics and atrazine adsorption capacity of co-pyrolysed and mixed biochars generated from corn straw and sawdust. Environ Res 172:561–568. https://doi.org/10.1016/j.envres.2019.03.010

Gao WR, Lin ZX, Chen HR, Yan SS, Huang Y, Hu X, Zhang S (2022) A review on N-doped biochar for enhanced water treatment and emerging applications. Fuel Process Technol 237:107468. https://doi.org/10.1016/j.fuproc.2022.107468

Gu SY, Zhang DF, Gao YQ, Qi RZ, Chen WF, Xu ZH (2021) Fabrication of porous carbon derived from cotton/polyester waste mixed with oyster shells: pore-forming process and application for tetracycline removal. Chemosphere 270:129483. https://doi.org/10.1016/j.chemosphere.2020.129483

Hernandes PT, Franco DSP, Georgin J, Salau NPG, Dotto GL (2022) Adsorption of atrazine and 2,4-D pesticides on alternative biochars from cedar bark sawdust (*Cedrella fissilis*). Environ Sci Pollut Res 29:22566–22575. https://doi.org/10.1007/s11356-021-17590-4

Hong MF, Zhang LM, Tan ZX, Huang QY (2019) Effect mechanism of biochar's zeta potential on farmland soil's cadmium immobilization. Environ Sci Pollut Res 26:19738–19748. https://doi.org/10.1007/s11356-019-05298-5

Hu XJ, Wang JS, Liu YG, Li X, Zeng GM, Bao ZL, Zeng XX, Chen AW, Long F (2011) Adsorption of chromium (VI) by ethylenediamine-modified cross-linked magnetic chitosan resin: isotherms, kinetics and thermodynamics. J Hazard Mater 185:306–314. https://doi.org/10.1016/j.jhazmat.2010.09.034

Islam A, Teo S, Chan E, Taufiq-Yap Y (2014) Enhancing sorption performance of surfactant-assistant CaO nanoparticles. RSC Adv 110:65127–65136

Ji RT, Wu YR, Bian YR, Song Y, Sun Q, Jiang X, Zhang LJ, Han JG, Cheng H (2021) Nitrogen-doped porous biochar derived from marine algae for efficient solid-phase microextraction of chlorobenzenes from aqueous solution. J Hazard Mater 407:124785. https://doi.org/10.1016/j.jhazmat.2020.124785

Jiang Z, Shao Q, Chu YX, An N, Cao B, Ren ZY, Li J, Qu JH, Dong MF, Zhang Y (2022) Mitigation of atrazine-induced oxidative stress on soybean seedlings after co-inoculation with atrazine-degrading bacterium *Arthrobacter* sp. DNS10 and inorganic phosphorus-solubilizing bacterium *Enterobacter* sp. P1. Environ Sci Pollut Res 30:30048–30061. https://doi.org/10.1007/s11356-022-24070-w

Kiran B, Kaushik A (2008) Chromium binding capacity of *Lyngbya putealis* exopolysaccharides. Biochem Eng J 38:47–54. https://doi.org/10.1016/j.bej.2007.06.007

Lee XJ, Ong HC, Gan YY, Chen WH, Mahlia TMI (2020) State of art review on conventional and advanced pyrolysis of macroalgae and microalgae for biochar, bio-oil and bio-syngas production. Energy Conv Manag 210:112707. https://doi.org/10.1016/j.enconman.2020.112707

Li JM, Jiang QM, Wei LS, Zhong LX, Wang XY (2020) Simple and scalable synthesis of hierarchical porous carbon derived from cornstalk without pith for high capacitance and energy density. J Mater Chem A 8:1469–1479. https://doi.org/10.1039/c9ta07864a

Li C, Li QY, Jiang YC, Shao YW, Gao GM, Zhang S, Xiang J, Hu S, Wang Y, Hu X (2023) Importance of oxidation reactions in creating pores in physical activation of biomasses. Chem Eng J 474:145748. https://doi.org/10.1016/j.cej.2023.145748

Liang Y, Zhao B, Yuan CQ (2022) Adsorption of atrazine by Fe-Mn-modified biochar: the dominant mechanism of π-π interaction and pore structure. Agronomy-Basel 12:3097. https://doi.org/10.3390/agronomy12123097

Liu GX, Bian YR, Jia MY, Boughner LA, Gu CG, Song Y, Sheng HJ, Zhao W, Jiang X, Wang F (2017) Effect of extracellular polymeric substance components on the sorption behavior of 2,2',4,4'-tetrabromodiphenyl ether to soils: kinetics and isotherms. Sci Total Environ 609:144–152. https://doi.org/10.1016/j.scitotenv.2017.07.089

Liu YY, Ma SQ, Chen JW (2018) A novel pyro-hydrochar via sequential carbonization of biomass waste: preparation, characterization and adsorption capacity. J Clean Prod 176:187–195. https://doi.org/10.1016/j.jclepro.2017.12.090

Llado J, Lao-Luque C, Ruiz B, Fuente E, Sole-Sardans M, Dorado AD (2015) Role of activated carbon properties in atrazine and paracetamol adsorption equilibrium and kinetics. Process Saf Environ Protect 95:51–59. https://doi.org/10.1016/j.psep.2015.02.013

Netto MS, Georgin J, Franco DSP, Mallmann ES, Foletto EL, Godinho M, Pinto D, Dotto GL (2022) Effective adsorptive removal of atrazine herbicide in river waters by a novel hydrochar derived from *Prunus serrulata* bark. Environ Sci Pollut Res 29:3672–3685. https://doi.org/10.1007/s11356-021-15366-4

Nguyen TB, Truong QM, Chen CW, Chen WH, Dong CD (2022) Pyrolysis of marine algae for biochar production for adsorption of ciprofloxacin from aqueous solutions. Bioresour Technol 351:127043. https://doi.org/10.1016/j.biortech.2022.127043

Ok YS, Lim JE, Moon DH (2011) Stabilization of Pb and Cd contaminated soils and soil quality improvements using waste oyster shells. Environ Geochem Health 33:83–91. https://doi.org/10.1007/s10653-010-9329-3

Poo KM, Son EB, Chan JS, Ren XH, Choi YJ, Chae KJ (2018) Biochars derived from wasted marine macro-algae (*Saccharina japonica* and *Sargassum fusiforme*) and their potential for heavy metal removal in aqueous solution. J Environ Manage 206:364–372. https://doi.org/10.1016/j.jenvman.2017.10.056

Rostami S, Jafari S, Moeini Z, Jaskulak M, Keshtgar L, Badeenezhad A, Azhdarpoor A, Rostami M, Zorena K, Dehghani M (2021) Current methods and technologies for degradation of atrazine in contaminated soil and water: a review. Environ Technol Innov 24:102019. https://doi.org/10.1016/j.eti.2021.102019

Rumschlag SL, Bessler SM, Rohr JR (2019) Evaluating improvements to exposure estimates from fate and transport models by incorporating environmental sampling effort and contaminant use. Water Res 156:372–382. https://doi.org/10.1016/j.watres.2019.03.038

Sajjadi B, Chen WY, Egiebor NO (2019) A comprehensive review on physical activation of biochar for energy and environmental applications. Rev Chem Eng 35:735–776. https://doi.org/10.1515/revce-2017-0113

Shi QQ, Wang YT, Zhang X, Shen BX, Wang FM, Zhang YF (2020) Hierarchically porous biochar synthesized with $CaCO_3$ template for efficient $Hg^0$ adsorption from flue gas. Fuel Process Technol 199:106247. https://doi.org/10.1016/j.fuproc.2019.106247

Tan XF, Liu SB, Liu YG, Gu YL, Zeng GM, Hua XJ, Wang X, Liu SH, Jiang LH (2017) Biochar as potential sustainable precursors for activated carbon production: Multiple applications in environmental protection and energy storage. Bioresour Technol 227:359–372. https://doi.org/10.1016/j.biortech.2016.12.083

Tao Y, Han SY, Zhang Q, Yang Y, Shi HT, Akindolie MS, Jiao YQ, Qu JH, Jiang Z, Han W, Zhang Y (2020) Application of biochar with functional microorganisms for enhanced atrazine removal and phosphorus utilization. J Clean Prod 257:120535. https://doi.org/10.1016/j.jclepro.2020.120535

Wang PP, Liu XG, Yu BC, Wu XH, Xu J, Dong FS, Zheng YQ (2020a) Characterization of peanut-shell biochar and the mechanisms underlying its sorption for atrazine and nicosulfuron in aqueous solution. Sci Total Environ 702:134767. https://doi.org/10.1016/j.scitotenv.2019.134767

Wang YF, Kang JM, Jiang SM, Li H, Ren ZY, Xu QB, Jiang Q, Liu WZ, Li RZ, Zhang Y (2020b) A composite of Ni-Fe-Zn layered double hydroxides/biochar for atrazine removal from aqueous solution. Biochar 2:455–464. https://doi.org/10.1007/s42773-020-00066-y

Wang CQ, Lin X, Zhang XX, Show PL (2024) Research advances on production and application of algal biochar in environmental remediation. Environ Pollut 348:123860. https://doi.org/10.1016/j.envpol.2024.123860

Wen YM, Wang SL, Shi ZY, Jin YH, Thomas JB, Azzi ES, Franzen D, Grondahl F, Martin A, Tang CC, Mu WZ, Jonsson PG, Yang WH (2022) Pyrolysis of engineered beach-cast seaweed: performances and life cycle assessment. Water Res 222:118875. https://doi.org/10.1016/j.watres.2022.118875

Xiang W, Zhang XY, Chen JJ, Zou WX, He F, Hu X, Tsang DCW, Ok YS, Gao B (2020) Biochar technology in wastewater treatment: a critical review. Chemosphere 252:126539. https://doi.org/10.1016/j.chemosphere.2020.126539

Yan SJ, Qu JH, Bi FX, Wei SQ, Wang SQ, Jiang Z, Wang L, Yu HW, Zhang Y (2022) One-pot synthesis of porous N-doped hydrochar for atrazine removal from aqueous phase: co-activation and adsorption mechanisms. Bioresour Technol 364:128056. https://doi.org/10.1016/j.biortech.2022.128056

Yang F, Sun LL, Xie WL, Jiang Q, Gao Y, Zhang W, Zhang Y (2017) Nitrogen-functionalization biochars derived from wheat straws via molten salt synthesis: an efficient adsorbent for atrazine removal. Sci Total Environ 607:1391–1399. https://doi.org/10.1016/j.scitotenv.2017.07.020

Yao S, Li XN, Cheng H, Zhang C, Bian YR, Jiang X, Song Y (2019) Resource utilization of a typical vegetable waste as biochars in removing phthalate acid esters from water: a sorption case study. Bioresour Technol 293:122081. https://doi.org/10.1016/j.biortech.2019.122081

Yi ZJ, Li C, Li QY, Zhang LJ, Zhang S, Wang S, Qin L, Hu X (2022) Influence of $CO_2$ atmosphere on property of biochar from pyrolysis of cellulose. J Environ Chem Eng 10:107339. https://doi.org/10.1016/j.jece.2022.107339

Yuan Y, Huang LJ, Zhang TC, Wang Y, Yuan SJ (2023) $CaCO_3$-ZnO loaded scrap rice-derived biochar for $H_2S$ removal at room-temperature: characterization, performance and mechanism. Fuel Process Technol 249:107846. https://doi.org/10.1016/j.fuproc.2023.107846

Zanli B, Tang W, Chen JW (2022) N-doped and activated porous biochar derived from cocoa shell for removing norfloxacin from aqueous solution: Performance assessment and mechanism insight. Environ Res 214:113951. https://doi.org/10.1016/j.envres.2022.113951

Zhao M, Ma X, Liao X, Cheng S, Liu Q, Wang H, Zheng H, Li X, Luo X, Zhao J, Li F, Xing B (2022) Characteristics of algae-derived biochars and their sorption and remediation performance for sulfamethoxazole in marine environment. Chem Eng J 430:133092. https://doi.org/10.1016/j.cej.2021.133092

Zheng W, Guo MX, Chow T, Bennett DN, Rajagopalan N (2010) Sorption properties of greenwaste biochar for two triazine pesticides. J Hazard Mater 181:121–126. https://doi.org/10.1016/j.jhazmat.2010.04.103